FINAL REPORT ADDENDUM

Environmental Fate and Exposure Assessment for Arsenic in Groundwater

SERDP Project ER-1374

JUNE 2010

Peggy O'Day
Virginia Illera
University of California, Merced

Front Matter

List of Tables

List of Figures

List of Acronyms

EXAFS – Extended X-ray absorption fine structure
LVR – Large volume reactor
MNA – monitored natural attenuation
SB – Sequential batch
SEM – Scanning electron microscopy
SSRL – Stanford Synchrotron Radiation Lightsource
XANES –X-ray absorption near edge spectroscopy
XAS – X-ray absorption spectroscopy
XRD – X-ray diffraction

Keywords

Arsenic sulfide, iron sulfide, X-ray absorption spectroscopy, monitored natural attenuation

Acknowledgments

This work was supported by SERDP Project #ER-1374. N. Rivera, S. Serrano, and D. Beals assisted with data collection and analysis. Portions of this research were carried out at the Stanford Synchrotron Radiation Lightsource, a national user facility operated by Stanford University on behalf of the U.S. Department of Energy, Office of Basic Energy Sciences.

Abstract

This one-year project extension was aimed at identifying and characterizing end-member As- and Fe- sulfide precipitates and co-precipitated As+Fe sulfide phases as potential sinks for As in sulfate-reduced environments. Precipitation experiments used starting solutions with As^{3+} (as arsenite, AsO_3^{3-}), sulfide (S^{2--}), and either Fe^{2+} or Fe^{3+}, and As-only or Fe-only end-members at pH 3 or 4, 6, and 8 and aged for up to 210 d. Products were characterized by synchrotron X-ray absorption spectroscopy (XAS) and by synchrotron and laboratory XRD. Results from precipitation experiments under strict anoxic conditions showed that the primary solid products at low pH (3, 4) were mixtures of amorphous-to-crystalline Fe and As sulfides, with no evidence for extensive solid solution. With starting solutions containing As^{3+} + Fe^{2+} + S^{2--}, mixtures of Fe or As sulfides, a green rust-type phase (Fe^{2+}, Fe^{3+}-hydroxide), and a fraction of As^{3+} bonded to oxygen formed at higher pH (6, 8). With starting solutions containing As^{3+} + Fe^{3+}+ S^{2--}, no As sulfide was precipitated and all As was identified as the arsenite species, probably present mostly as a sorbed complex. Iron precipitated as a mixture of Fe sulfide and an Fe(III)-oxide phase that with aging formed poorly crystalline hematite. Precipitates were initially amorphous to X-ray diffraction and became more crystalline with aging for end members, but the rate of transformation of Fe sulfides and oxides from amorphous to crystalline was generally much slower (weeks to months) when As was present in solution. Characterization of precipitation products by XAS at aging times up to one month indicated that that the local structure around Fe or As was indicative of the final solid products after 210 d of aging. These data suggest that small (perhaps nano-to-micro-meter sized) particles are nucleating on short time scales consistent with overall thermodynamic stability, but that ripening to long-range crystallographic ordering are inhibited when both Fe and As are present in solution.

Objective

This project was a one-year extension of Project ER-1374 ("Environmental Fate and Exposure Assessment for Arsenic in Groundwater"). The scope of work addressed the following data gaps related to the long-term stability of As- and Fe-bearing sulfide phases, as end-members and mixtures, and their potential for As release in monitored natural attenuation (MNA) settings.

Task 1: Identification, characterization, and solubility of end-member As- and Fe- sulfide precipitates and co-precipitated As+Fe sulfide phases.

-- Subtask 1: Synthesis and spectroscopic characterization of As-sulfide and Fe-sulfide precipitates at circum-neutral pH to establish the composition and structure of newly precipitated end-member phases.

-- Subtask 2: Synthesis and spectroscopic characterization of As+Fe-sulfide of co-precipitated phases and solutions at circum-neutral pH to establish the identity of newly formed phases (i.e., end-member versus solid-solution) and their apparent solubility compared with thermodynamic solubilities of crystalline polymorphs.

Task 2: Dissolution rate experiments with precipitated As-sulfides with abiotic oxidants (O_2, Fe(III)).

-- Subtask 1: Measurement of dissolution rates of precipitated As-sulfides (in a quartz matrix) using flow-through columns.
-- Subtask 2: Characterization of speciation in effluent solutions and changes in sulfide phases after dissolution experiments.

Background

The effective application of monitored natural attenuation (MNA) as a remediation approach for arsenic-contaminated sites requires knowledge of sources and sinks for arsenic (Hering et al., 2009). The two primary modes of partitioning from aqueous to solid phases are sorption and precipitation/co-precipitation. Much attention has focused on sorption processes, which are relatively fast, often controlled by pH and competitive ions, and can be quantified from an equilibrium standpoint. Thus, one of the key knowledge gaps for solid-phase release of arsenic is the identity, solubility, and rates of dissolution of arsenic-bearing phases, particularly of recently precipitated As-sulfide phases, which typically form in natural environments as a result of biological sulfate reduction (Oremland et al., 2002; Stolz and Oremland, 1999). Although most freshwater sites in general contain low dissolved sulfate, any sulfate that enters a reducing, organic-rich system is rapidly reduced to sulfide by microbial action and can precipitate as Fe and/or As sulfide phase once solubility is exceeded. Precipitation of these phases has been documented in laboratory experiments and fields sites to occur on timescales of hours to months (Rickard and Luther, 2007). Precipitation of sulfide, in most cases dominated by iron but potentially associated with other elements, is an effective sink for arsenic. Our prior studies of freshwater aquifer sediments and tidal marsh areas (O'Day et al., 2004b; Root et al., 2007; Root et al., 2009), as well as work by other groups in aquifer and near-surface sediments, suggests that biogenic sulfide precipitation has been overlooked as sink for arsenic.

This study examined the abiotic precipitation of As and Fe sulfide solids as individual phases and in mixed As+Fe systems as a function of pH in batch experiments as a model system for determining the phases, composition, structure, and crystallinity immediately after precipitation and with aging for weeks to months. In addition, preliminary experiments we done to examine the dissolution of As sulfide precipitates in flow-through experiments.

Materials and Methods

1. Batch and Reactor Experiments

Sulfide precipitates were made by two methods, serial batch (SB) experiments, in which solutions were mixed in a series of 50 ml polypropylene tubes and analyzed as a function of aging time, and in a gas-tight large volume reactor (LVR), consisting of a 500-ml glass round-bottom flask with ground glass entry ports. The ports were fitted with (1) gas in-flow and out-flow tubes to maintain constant reduced conditions using a 95%N_2/5%H_2 gas mixture; (2) a sampling port; (3) a motor of a conventional laboratory stirrer connected with a rotating shaft through a rubber stopper in a gas-tight manner; and (4) pH and ORP electrodes. Out-flow gas was trapped by bubbling through a 0.1 M silver nitrate solution in order to capture any exsolved $H_2S(g)$. Temperature was kept at 25°C and a constant flow of gas through the solutions was maintained during the experiment (except when sampling and taking pH and ORP measurements). To avoid any oxygen contamination, the SB and LVR experiments were kept inside a N_2 – atmosphere glove box (Coy Products) under strict anaerobic conditions.

Before each experiment, fresh stock solutions of As^{3+}, S^{2-}, and Fe^{2+} or Fe^{3+} were made with deoxygenated water, which was prepared by bubbling purified N_2 in high purity water (18 MΩ-cm) for at least one day. The Fe^{3+} salt was dissolved in deoxygenated water containing 0.01 M HCl (to prevent iron hydroxide precipitation). All solutions were prepared in the N_2 – atmosphere glove box. Reagent-grade chemicals were used in all experiments. Table 1 summarizes reagents and conditions for the precipitation experiments.

In addition to As+Fe mixtures, end-member amorphous arsenic sulfide phases were synthesized, including orpiment (As_2S_3) and amorphous and crystalline iron sulfide phases (mackinawite (FeS), greigite (Fe_3S_4), and pyrite (FeS_2)). Iron, arsenic, and sulfur from different salts (chloride, ammonium sulfate, sulfate) were tested in the synthesis at different temperatures and pH conditions to evaluate potential differences in reaction products. These experiments were done at 25°C in 50 or 60 ml polypropylene tubes in an N_2 – atmosphere glove box under strict anaerobic conditions.

Experiments at higher temperatures (100-190°C), were aged in 50 ml Pyrex glass tubes with screw caps in a laboratory oven. At the end of the reaction period, tubes were transferred to a glove box, keeping anaerobic conditions during the whole process. The highest temperature (190°C) was chosen in order to attempt greigite (Fe_3S_4) synthesis (Table 1, exp. 2.2. at 190°C). After mixing 0.15 M Mohr's salt ($Fe(NH_4)_2(SO_4)_2 \cdot 6H_2O$) and 0.2 M sodium sulfide, the suspension was heated to 190°C for 1 hour. Then without delay, the 50 ml Pyrex glass tube was transferred from the laboratory oven to the glove box and plunged into cold water (4°C) to quench the suspension, which should produce pure greigite according to (Uda, 1967) and (Yamaguch and Wada, 1972). However, in this case, a mixture of mackinawite and greigite was obtained (see below), rather than a pure greigite phase.

For SB experiments when Fe^{2+} was used, 16.5 ml of 1.0 M $Fe(NH_4)_2(SO_4)_2$ was added to 18 ml of 0.6 M $AsNaO_2$ and to 16.5 ml of 1.0 M $Na_2S \cdot 9H_2O$, to a final volume of 55 ml. When Fe^{3+} was used, 3 ml of 1.0 M $FeCl_3$ was added to 6.5 ml of 0.6 M $AsNaO_2$ and to 6 ml of 1.0 M of NaSH, to a final volume of 48 ml. Deoxygenated water was added to complete the final volumes (55 and 48 ml, respectively), and the final molar concentrations were 0.3 M Fe^{2+}, 0.3 M S^{2-}, and 0.2 M As^{3+} (mixtures with Fe^{2+}) and 0.06 M Fe^{3+}, 0.12 M S^{2-}, and 0.08 M As^{3+} (mixtures with Fe^{3+}).

For LVR experiments, equal volumes (100 ml each) of 1.2 M Fe^{2+} or Fe^{3+} and 1.2 M S^{2-} solutions, and 80 ml of 1.0 M As^{3+} solution were directly mixed in the reactor with vigorous stirring, and then diluted further with deoxygenated water to obtain final molar concentrations of 0.3 M Fe^{2+} or Fe^{3+}, 0.3 M S^{2-}, and 0.2 M As^{3+}. The pH of the reaction solutions (SB and LVR) was controlled by small additions of concentrated HCl or NaOH. The pH (measured using an Orion double junction pH electrode) and ORP were monitored throughout each experiment.

The SB samples were shaken manually for a few minutes after solutions were mixed, and then stored in the glove box for aging 7 and 30 d (no rotation during aging). The LVR was stirred continuously at ~1000 rpm. At different time intervals (4 hr, 12 hr, 1 d), 30 ml aliquots were extracted from the LVR. After 1 d, the rest of the suspension was transferred from the reactor vessel to individual 50 ml polypropylene tubes and aged longer (7, 120, and 210 d). After each aging time, a tube (SB or LVR) was sacrificed for analysis. For aqueous concentrations, supernatant solutions (10 ml) were filtered through polypropylene membrane filters (< 2 μm) and analyzed for total iron, arsenic, and sulfur by ICP-OES and/or ICP-MS.

Samples were kept as a suspension and aliquots (~5-10 ml) were centrifuged (at 15000 rpm for 10 min) just prior to analysis of solid-phase precipitates by X-ray diffraction (XRD) or

X-ray absorption spectroscopy (XAS). Solid-phase precipitates aged for 120 d (LVR) were washed with deoxygenated, deionized water, and then a phosphate extraction was performed (0.005 M NaH_2PO_4) to estimate the adsorbed As fraction. Also, a fraction of the LVR 120 d washed precipitates was dried at ambient temperature inside the N_2 – atmosphere glove box, and later analyzed by scanning electron microscopy (SEM).

For micro X-ray fluorescence (μXRF), another fraction of the dried LVR 120 d (pH 6) precipitates was made into thin sections. After drying, samples were embedded in Epotek 301 resin (Epoxy Technologies, Inc.) inside the N_2 – atmosphere glove box. Particles were dispersed at the bottom of square polyethylene "peel-a-way" embedding mold (Polyscience, Inc.; 22 mm x 22 mm square and 20 mm deep). The mixed epoxy was poured over the solids to cover about 0.5 cm (the container should be less than half full to prevent possible overflow when the epoxy foams). The embedding molds were then placed in a vacuum desiccator and evacuated for 3 days to cure. After curing, the resin pucks were easily removed from the molds and sent to Spectrum Petrographics, Inc. for cutting into standard 30-μm, double-polished petrographic thin sections mounted on high purity fused quartz slides with superglue. Low oxygen and temperature conditions were requested to prevent possible changes in oxidation state resulting from processing.

2. Dissolution Experiments

Dissolution of precipitated arsenic sulfide, identified as amorphous As_2S_3 (local structure orpiment-like), was examined using small flow-through column experiments with and without dissolved O_2(aq). Sulfide particles were mixed with ground quartz to provide a non-reactive matrix and dispersion of particles. Columns were run for up to 500 pore volumes in small-volume (3 ml) reactors under conditions of fully oxygen saturated (equivalent to ambient air) and low O_2(aq) (solutions purged with N_2). Column effluent was monitored for pH and oxidation-reduction potential (ORP) by in-line electrode. Effluent solutions were measured for total dissolved As and S by either ICP-OES or ICP-MS, depending on the concentration.

3. Characterizations of Solutions and Reaction Products

a. Chemical Analyses

Element concentrations in supernatant solutions were measured by ICP-OES (Perkin-Elmer Optima 4000 DV) for As, Fe, and total S. ICP-MS (Agilent 7500cs) was used when As and Fe concentrations in solution were lower than the ICP-OES detection limit. Detection limits (DL) for As, Fe and S by ICP-OES were 10 ppb, 2 ppb and 100 ppb, respectively; DL for As and Fe by ICP-MS were 0.02 ppb and 0.2 ppb, respectively.

b. Synchrotron X-ray Data Collection and Analysis

Arsenic and Fe K-edge X-ray absorption spectra were collected at the Stanford Synchrotron Radiation Lightsource (SSRL) on wiggler beamline 11-2 or 4-1 under dedicated conditions (3 GeV, 80-150 mA). Sulfur K-edge spectra were collected at SSRL on wiggler beamline 4-3 (3 GeV, 80-150 mA). For As and Fe, samples were diluted with boron nitride. For S analysis, samples were spread as very thin films on layers of sulfur-free tape. Arsenic and Fe EXAFS spectra (to k = 12-14 $Å^{-1}$) were collected using Si(220) monochromator crystals in either transmission using gas-filled ion chambers, or fluorescence with a 13-element in beamline 4-1 and 30-element Ge detector in beamline 11-2, with the sample held at in a liquid He cryostat (temp. = 4-8 K). Beam size at BL 11-2 (focused beam) was 0.5 x 3.0 mm; beam size at BL 4-1

(unfocused beam) was 4 x 18 mm (hutch slit size was adjusted between 2 x 12 mm to 1 x 10 mm, depending on the sample). For S XAS, a Lytle detector was used with the sample at room temperature. Beam size at BL 4-3 (unfocused beam) was 3 x 16 mm (hutch slit size was adjusted to 2 x 10 mm). Beam energy was calibrated on As foil (main edge inflection) at 11,867 eV, on Fe foil (first edge inflection) at 7112 eV, and for S, with a thiosulfate standard (first maximum peak) at 2472 eV. For each element, 3-6 scans were collected and averaged.

Absorption data were analyzed using the computer packages Sixpack (Webb, 2005) and EXAFSPAK (George and Pickering, 2000). Background was subtracted from averaged spectra by extrapolation from the pre-edge region and spectra were normalized to the average post-edge step height. XANES spectra (either normalized or first-derivative normalized spectra) were fit using linear least-squares combinations of end-member and reference compound spectra. EXAFS spectra were fit by non-linear least-squares methods in k-space and the entire k-range was used in the fit (i.e., no reverse Fourier filtering was done). Theoretical phase-shift and amplitude reference functions were calculated with the program Feff 8.4 (Ankudinov et al., 1998). In fits to As and Fe EXAFS spectra, either backscatterer number (N) or Debye-Waller factor (σ^2) were varied in fits (because of the strong co-variance between N and σ^2), together with interatomic distance (R). Difference in threshold energy (ΔE_0) between experimental data and reference functions was treated as a single adjustable parameter for all atomic shells associated with either S or O first-shell backscatterers. For As EXAFS of As^{3+} + Fe^{2+} sulfides, σ^2 was fixed on a value estimated from (O'Day et al., 2004b), while As EXAFS fits of As^{3+} + Fe^{3+} sulfides used σ^2 for As^{3+} sorbed to iron oxide surfaces taken from (Root et al., 2009). For Fe EXAFS end-members, N was fixed based on crystallographic values from literature and σ^2 was varied (Lennie and Vaughan, 1996; O'Day et al., 2004b). Estimated errors based on empirical fits to reference compounds are: first shell: R ± 0.01 Å; N ± 10%; greater than first shell: R ± 0.02 Å; N ± 30%; σ^2 ± 30% (O'Day et al., 2004a; O'Day et al., 2004b).

Synchrotron X-ray diffraction data were collected at SSRL on beamline 11-3, in transmission mode with the radiation source at λ = 0.9753 Å using Si(111) monochromator crystals with a focused spot size of 150 μm and a MAR345 image plate detector. Detector geometry, X-ray wavelength, and diffractograms were calibrated with a LaB_6 standard and converted to wavelength using a non-linear curve fit and Bragg fit equations. The Fit2D software package version V12.077 (Hammersley, 1997) was used for radial averaging of the Laue diffraction pattern. Data analysis and peak identification was performed using the Jade software package (MDI Products) with ICCD PDF-2 database.

Microfocused X-ray fluorescence maps were collected at SSRL on beamline 2-3 (beam size 2 x 2 μm) with Si(111) monochromator crystals and K-B microfocusing mirrors. Fluorescence was collected with a Ge3 detector with 1 channel. Iron fluorescence maps and energy difference maps were collected on particles embedded in thin sections. The maps were constructed by scanning the particle at different energies (7113, 7126, 7129 and 7140 eV), which correspond to maximum absorption in the edge region for different iron mineral phases or species. The maps were analyzed using SMAK version 0.51 (Webb, 2006). The resultant tricolor maps showed the calculated distribution of the element species or mineral phases of the particle.

c. Laboratory X-ray Diffraction

Diffractograms were collected on a laboratory X-ray diffractometer (PanAnalytical X'Pert PRO with an ultra-fast X'Celerator detector). Samples were mounted on zero-

background Si holders and scanned from 4 degrees to 75 degrees 2θ at 0.01-degree 2θ steps with a Co K-alpha source (λ = 1.78 Å). Quantitative-XRD phase analysis was performed using the Rietveld module in the X'Pert HighScore Plus software with the ICDD PDF-2 database.

d. Scanning Electron Microscopy (SEM)

Precipitates were mounted on Al-alloy stub mounts with double-stick carbon tape and gold-coated. Images were collected at the Imaging and Microscopy Facility (UC Merced) using a FEI Quanta 200 E-SEM with a tungsten filament operating at 15-25 kV and a working distance of 5-10 mm. Element fluorescence was measured with EDAX Genesis energy-dispersive X-ray spectrometer.

Results

1. End-member As-Sulfide and Fe-Sulfide Precipitates

In end-member precipitation experiments, X-ray diffraction showed that reaction products are mostly amorphous when initially formed, but convert to more crystalline phases after aging for hours to days. X-ray diffractograms (Fig. 1) showed that mackinawite (FeS) was the main phase precipitated from Fe^{2+} + S^{2-} solutions at pH 6 and 8 at 25 °C (exp. 2.1). Quantitative analysis by Fe X-ray absorption spectroscopy showed that the local bonding around Fe matched the mackinawite structure in mostly amorphous precipitates aged for 4 hours (Table 2). With further aging for 7 days, second-neighbor backscattering from S and Fe atoms increased in amplitude, consistent with an increasingly crystalline structure as noted in XRD. Scanning electron micrographs of precipitates showed a platy morphology typical of mackinawite (Fig. 2). The same experiment was done at higher temperatures (exp. 2.1: 60 and 100°C). At higher temperature, the XRD pattern indicated a more crystalline mackinawite (data not shown).

Similar experiments with slightly different Fe^{2+}/S^{2-} ratios were done at 100 and 190 °C (exp. 2.2.) and solids were quenched at the end of the reaction time. These experiments produced mostly mackinawite, with evidence from XRD for a small fraction of greigite (Fe_3S_4) (Fig. 1). At pH 3 and room temperature, greigite with a small fraction of pyrite was precipitated from Fe^{2+} + S^{2-} solutions when the molar ratio of sulfur to iron was 2:1 (exp. 2.5). The addition of elemental S (in the form of sulfur powder) to Fe^{2+} + S^{2-} solutions at 25 °C produced an amorphous solid with emergent XRD reflections of pyrite (FeS_2) after 7 d of aging at pH 4 (exp. 2.3) In synthesis experiments with Fe^{3+}+ S^{2-} at pH 3, pyrite was the only crystalline product identified (exp. 2.7); precipitates at higher pH (6, 8) were X-ray amorphous. Initial solutions with Fe^{3+}+ HS^- at pH 4 (exp. 2.6) produced a more complex mixture of pyrite, greigite, and mackinawite based on XRD reflections (Fig. 1). For precipitates from Fe^{3+} solutions, Fe XANES showed that pyrite formed at pH 3, consistent with XRD results (Table 2). At pH 6, Fe-XAS indicated amorphous mackinawite.

Mixtures of As^{3+} + S^{2-} at pH 4 produced mostly amorphous solids with weak reflections in X-ray diffractograms associated with orpiment (exp. 1.1) within 1 day of precipitation. Arsenic XAS indicated that the local bonding structure around As was similar to the orpiment (As_2S_3) structure (Table 3).

2. As^{3+} + Fe^{2+} Sulfide Precipitates

Precipitation of solids from As^{3+}+ Fe^{2+} + S^{2-} solutions at pH 4 and 6 were mostly X-ray amorphous by both synchrotron and laboratory XRD at all aging times (~4 hours to 210 days) (Fig. 3). At pH 6 after 210 d of aging (exp. 4.1), incipient peaks corresponding to mackinawite are discernable in XRD. Analysis of Fe XANES at pH 6 (Fig. 4; Table 4) indicated a mixture of an Fe-sulfide phase that was best fit with amorphous mackinawite and a green rust-type phase in roughly equal amounts. Fluorescence mapping of Fe oxidation states using a microfocused synchrotron X-ray beam showed particles with an Fe sulfide core and green rust around the rims, and a smaller amount of Fe(III) oxide on the edges that is probably a result of oxidation in air during data collection (Fig. 5). Fits to As XANES and EXAFS for both SB and LVR experiments (Fig. 6; Table 3; Table 5) indicated that As was mostly present as a sulfide with a smaller fraction of As bonded to O (~17-34%). Quantitative analysis yielded interatomic distances that corresponded to a local atomic structure similar to orpiment (first shell As-S = 2.27±0.01 Å), and a smaller fraction of As^{3+} bonded to oxygen (first shell As^{3+}-O = 1.79 ± 0.01 Å) (Table 3). Scanning electron micrographs showed larger particles with plate-like morphologies with smaller particles on their surfaces, as well as particle aggregates (Fig. 2). Extraction of LVR precipitates aged for 120 d by a weak phosphoric acid extraction removed 21% of the total As in the sample (Fig. 7) compared with 2% of total iron and 6% of total sulfur. The magnitude of the As^{3+}-O peak in the EXAFS correspondingly decreased after extraction with phosphate. Analysis of S XANES indicated a mixture of amorphous orpiment and mackinawite, consistent with the As and Fe XAS results, and showed no evidence for oxidation of sulfide to sulfate (Fig. 8; Table 6). Collectively, these observations indicate that the fraction of As^{3+} associated with oxygen is most likely a sorbed fraction, and XANES spectra could be fit with a reference spectrum of As^{3+} sorbed to a green rust phase.

At pH 8, precipitates appeared mostly amorphous by XRD at shorter aging times, with incipient reflections present at 7 d that corresponded most closely to realgar (AsS) (Fig. 3). At 210 d, XRD reflections showed sharper peaks indicative of crystalline realgar. Similar to results at pH 6, Fe XANES indicated a mixture of mackinawite (53%) and a green rust phase (40%) (Table 4). Analysis of As XANES and EXAFS showed that As was associated with a sulfide phase corresponding to the local structure of realgar and As^{3+} bonded to oxygen that was fit in the As XANES with As^{3+} sorbed to green rust (Fig. 6; Table 3; Table 5). The As^{3+}-oxygen fraction comprises a larger proportion of the As spectrum at pH 8 than at pH 6 (about 90%) by the XANES fit results. However, extraction of solids with phosphoric acid solution removed only 12% of total As, <1% of total Fe, and 5% of total S (Fig. 7), suggesting that the As^{3+}-oxygen fraction may be partially incorporated into solids rather than sorbed. The S XANES spectra were well fit with a mixture of realgar and mackinawite, and showed no evidence for sulfur oxidation (Fig. 8). *In situ* measurements of fluid pH and Eh in the LVR during exp. 4.1 at 7 and 120 d indicated more reduced conditions at pH 8 (negative ORP) than at pH 6 (positive ORP) (Table 7).

3. As^{3+} + Fe^{3+} Sulfide Precipitates

Similarly to the As^{3+} + Fe^{2+} system, precipitates were amorphous to XRD at shorter aging times, with peaks in the diffractograms emerging after 210 d of aging (Fig. 3). At pH 6, peaks associated with mackinawite were identified. The Fe XAS data indicated the presence of an Fe sulfide phase corresponding to mackinawite and an Fe(III) oxide phase that was best fit with a reference spectrum of crystalline hematite (Fe_2O_3) in approximately equal fractions (Fig. 9;

Table 2; Table 4). Microfocused fluorescence difference mapping of Fe oxidation states showed that particles were mixtures of mackinawite and an Fe(III)-oxide (Fig. 5). Arsenic XAS indicated the formation of an orpiment-type phase with a fraction of As^{3+} coordinated by oxygen that was fit with a reference spectrum of As^{3+} sorbed to Fe(III) oxide that comprised over 70% of the spectral amplitude (Fig. 10; Table 3; Table 5). Sulfur XANES was well fit with a mixture of half orpiment and half mackinawite, and no evidence for sulfate (Fig. 8; Table 6). Extraction of solids with phosphoric acid solution removed 31% of total As, <1% of total Fe, and 12% of total S (Fig. 7).

At pH 8, XRD shows small reflections that corresponded most closely to hematite (Fe_2O_3). Fits to Fe XANES and EXAFS indicated the presence of a mackinawite-type Fe sulfide phase and an Fe(III)-oxide phase that could be fit with a hematite spectrum. Quantitative fits to As XANES and EXAFS indicated no As sulfide and only As^{3+} coordinated by oxygen that was fit as a surface complex sorbed to Fe(III)-oxide (Fig. 10; Table 3; Table 5). Phosphate extraction results showed 35% removal of total As, 6% removal of total Fe, and 21% removal of total S (Fig. 7), consistent with a large fraction of sorbed As^{3+} bonded to oxygen. The sulfur XANES spectrum showed that only mackinawite was present, with no evidence for sulfate (Fig. 8; Table 6).

4. Arsenic Sulfide Dissolution Experiments

Exploratory experiments were conducted using a flow-through system to measure dissolution of amorphous orpiment-type As sulfide in the presence and absence of dissolved O_2 to simulate dissolution under oxic and suboxic conditions. Initial results of dissolution experiments with influent solutions buffered at pH 8 in the presence of dissolved O_2 (DO = 94%) showed that total As and S effluent concentrations fell to steady state after about 45 pore volumes of flushout (Fig. 11). In the absence of dissolved O_2 (DO = 0%) at pH 8, effluent concentrations reached steady state after about 20 pore volumes of flushout. The difference between the two experiments, however, may be due to differences in column packing and flow rather than a reflection of change in dissolution mechanism. In both experiments, the ratio of total S to As was slightly higher than expected for stoichiometric dissolution of $As_2S_3(s)$, about 2-2.5 rather than a stoichiometric ratio of 1.5. This result may indicate some re-adsorption of As at this pH. Initial attempts to determine As and S speciation in effluent solutions using ion chromatography coupled to ICP-MS indicated mostly reduced species, but definitive peak assignments were precluded by the presence of multiple peaks in chromatographs that probably correspond to mixtures of arsenite, thioarsenite, and polysulfide species.

Discussion

Results from the sulfide precipitation experiments under strict anoxic conditions showed that the primary solid products are mixtures of Fe and As sulfides at low pH (3, 4), and mixtures of Fe or As sulfides with more oxidized Fe oxide products at higher pH, in general agreement with thermodynamic predictions. In general, precipitates were initially amorphous to X-ray diffraction and became more crystalline with aging. However, the rate of transformation of Fe sulfides from amorphous to crystalline was strongly influenced by the presence of As in solution. In As-free solutions, crystalline products were produced within hours to days, whereas in solutions with As present, several months of aging were required before reflections emerged in diffractograms. Evidence from X-ray absorption spectroscopy, however, indicated that the local

structure around Fe or As was indicative of the final product after aging. These data suggest that small (perhaps nano-to-micro-meter sized) particles are nucleating on short time scales, but that organization of long-range crystallographic structures are inhibited when both Fe and As are present in solution.

With starting solutions of As^{3+}+ Fe^{2+} + S^{2-}, reaction products at pH 6 were mixtures of orpiment, mackinawite, and a green-rust-type phase (GR), with variable fractions of As^{3+} ligated by oxygen, probably as a sorbed complex. In none of the experiments was the presence of sulfate detected by S XANES, even in experiments in which GR comprised a significant fraction of the Fe precipitation products. Therefore, it is most likely that the GR phase that formed was a fougerite-type hydroxide GR (e.g., Fe^{II},$Fe^{III}(OH)_5$ or Fe^{II}_2 $Fe^{III}(OH)_7$) (Bourrie et al., 1999; Bourrie et al., 2004). Structural analysis from As, Fe, and S XAS data showed no evidence for extensive solid solution between As and Fe sulfides. At pH 8, reaction products were realgar, mackinawite, and a green-rust-type phase (GR), with variable fractions of As^{3+} ligated by oxygen. Given that the starting solution contained As, Fe, and S in their most reduced forms, the presence of more oxidized products at higher pH reflects the increasing hydrolysis of water and the ability of Fe to readily oxidize.

The standard state (25 °C, 1 bar, infinite dilution) pK_{a1} for $H_2S(aq)$ is 6.98. The pK_{a2} is less well constrained but estimated to be > 18 (Rickard and Luther, 2007). Therefore, sulfide reactions in aqueous solutions under most natural pH conditions will involve the species $H_2S(aq)$, HS^-, and potentially polysulfide species, depending on the total sulfide concentration, rather than the species S^{2-} (Rickard and Luther, 2007). Near circum-neutral pH, the reaction for the precipitation of mackinawite (FeS(m)) can be written

$$Fe^{2+} + HS^- = FeS(m) + H^+$$

or at low pH as

$$Fe^{2+} + H_2S = FeS(m) + 2H^+$$

which involves no change in formal oxidation state of Fe or S. In natural aqueous solutions, As^{3+} is present mostly as the arsenite species H_3AsO_3 (also written as $As(OH)_3$) with a pK_{a1} of 9.23. Therefore, the precipitation of orpiment ($As_2S_3(o)$) can be written:

$$2H_3AsO_3 + 3HS^- + 3H^+ = As_2S_3(o) + 6H_2O$$

Formally, there is no change in As or S oxidation state, but this reaction is more favored at lower pH whereas the mackinawite reaction is more favored at high pH. Orpiment is thermodynamically unstable above pH ~ 6-7, depending on total As and S activities (Nordstrom and Archer, 2003), but recent theoretical and experimental studies suggest that aqueous thioarsenite species are stable at high dissolved sulfide concentrations (Helz and Tossell, 2008; Vlassopoulos et al., 2010). The formation of a GR-type phase implies a partial oxidation of Fe^{2+} to Fe^{3+}, which can be written as a half-electron reaction with a free electron:

$$2Fe^{2+} + 5H_2O = (Fe^{2+}, Fe^{3+})(OH)_5(GR) + 5H^+ + 1e^-$$

Formation of GR-type phases is favored at higher pH and driven by hydrolysis. In these simplified experimental systems using a formal oxidation state approach, it is not immediately apparent which species is undergoing reduction in order to couple to the Fe oxidation reaction involved in GR formation. The assignment of formal oxidation states to sulfide species is not physically realistic given the covalent nature of the chemical bonds. Above pH 7 pH, both H_2O and H_2S are increasingly deprotonated, which stabilizes more oxidized species at higher pH.

The formation of realgar (written as either AsS(r) or As_4S_4(r)) from arsenite and sulfide starting solutions implies a formal oxidation state change in either As or S. If sulfide is assumed to retain its formal oxidation state of S^{2-}, then As can be assigned a formal reduction from As^{3+} to As^{2+} (written as a half-electron reaction):

$$H_3AsO_3 + HS^- + 2H^+ + 1e^- = AsS(r) + 3H_2O$$

Formation of realgar as a reduction reaction indicates that electron transfer may be coupled to an oxidation reaction such as the oxidation of Fe^{2+} (written as a half-electron reaction):

$$Fe^{2+} = Fe^{3+} + 1e^-$$

This simplified analysis explains the coexistence of realgar with more oxidized Fe precipitates at higher pH. It should be noted that these types of electron transfer reactions may be occurring on particle surfaces rather than in solution, as suggested by microfocused synchrotron X-ray fluorescence imaging.

With starting solutions of As^{3+}+ Fe^{3+} + S^{2-}, reaction products reflect more oxidized initial conditions with the presence of Fe^{3+}. At both pH 6 and 8, mackinawite precipitated, indicating reduction of Fe^{3+}. Mackinawite coexists with an Fe(III) oxide that is initially amorphous but ages to poorly crystalline hematite. At pH 8, As is present only as As^{3+} ligated to oxygen (presumably sorbed), reflecting the stability of mackinawite and not orpiment at high pH. Even with these more oxidized starting solutions, the presence of As^{5+} (as arsenate) was not detected by As XAS, nor was any sulfate detected by S XAS.

Conclusions and Implications for Future Research

These studies demonstrate that sulfide phases can be a sink for As under sulfate-reduced conditions, particularly at low pH. With increasing pH (above pH ~7) the higher stability of Fe sulfide phases, particularly mackinawite, compared with As sulfide phases results in precipitation of Fe and sulfide from solution with no evidence for substantial incorporation of As into Fe sulfides. At pH 6 and 8, Fe phases are a mixture of sulfide and green-rust-type phases when starting solutions contain Fe^{2+}, and sulfide and Fe(III)-oxide when initial solutions have Fe^{3+}. With increasing pH, a larger fraction of As is present as arsenite ($H_xAsO_3^{x-3}$) rather than As sulfide, possibly as a sorbed complex, which may make it susceptible to desorption. The assemblage of phases and species observed as a function of initial solution composition and pH are broadly consistent with thermodynamic predictions, although solubilities of amorphous and poorly crystalline solids, particularly sulfide phases, are not well known (Helz and Tossell, 2008; Rickard and Luther, 2007). Future work will quantitatively analyze the thermodynamic relationships among product phases and assess potential refinement of solid-phase solubilities based on measurements of dissolved concentrations.

References

Ankudinov, A. L., Ravel, B., Rehr, J. J., and Conradson, S. D. (1998) Real-space multiple-scattering calculation and interpretation of x-ray-absorption near-edge structure. *Phys. Rev. B* **58**, 7565-7576.

Arakaki, T. and Morse, J. W. (1993) Coprecipitation and adsorption of Mn(II) with mackinawite (FeS) under conditions similar to those found in anoxic sediments. *Geochim. Cosmochim. Acta* **57**, 9-14.

Bourrie, G., Trolard, F., Genin, J. M. R., Jaffrezic, A., Maitre, V., and Abdelmoula, M. (1999) Iron control by equilibria between hydroxy-Green Rusts and solutions in hydromorphic soils. *Geochim. Cosmochim. Acta* **63**, 3417-3427.

Bourrie, G., Trolard, F., Refait, P., and Feder, F. R. (2004) A solid-solution model for Fe(II)-Fe(III)-Mg(II) green rusts and fougerite and estimation of their Gibbs free energies of formation. *Clays Clay Min.* **52**, 382-394.

Eary, L. E. (1992) The solubility of amorphous As2S3 from 25 to 90-degrees-C. *Geochim. Cosmochim. Acta* **56**, 2267-2280.

Elliott, N. (1960) Interatomic distances in FeS2, CoS2, AND NiS2. *J. Chem. Phys.* **33**, 903-905.

Gallegos, T. J., Hyun, S. P., and Hayes, K. F. (2007) Spectroscopic investigation of the uptake of arsenite from solution by synthetic mackinawite. *Environ. Sci. Technol.* **41**, 7781-7786.

George, G. N. and Pickering, I. J. (2000) EXAFSPAK: A suite of computer programs for analysis of X-ray absorption spectra. Stanford Synchrotron Radiation Laboratory.

Hammersley, A. P. (1997) FIT2D: An Introduction and Overview. ERSF Report 97HA02T.

Helz, G. R. and Tossell, J. A. (2008) Thermodynamic model for arsenic speciation in sulfidic waters: A novel use of ab initio computations. *Geochim. Cosmochim. Acta* **72**, 4457-4468.

Hering, J. G., O'Day, P. A., Ford, R. G., He, Y. T., Bilgin, A., Reisinger, H. J., and Burris, D. R. (2009) MNA as a remedy for arsenic mobilized by anthropogenic inputs of organic carbon. *Ground Water Monitor. and Remed.* **29**, 84-92.

Lennie, A. R. and Vaughan, D. J. (1996) Spectroscopic studies of iron sulfide formation and phase relations at low temperatures. In: Dyar, M. D., McCammon, C., and Schaefer, M. W. (Eds.), *Mineral Spectroscopy: A Tribute to Roger G. Burns*. The Geochemical Society.

Mullen, D. J. E. and Nowacki, W. (1972) Refinement of crystal-structures of realgar, AsS and orpiment, As2S3. *Z. Kristall.* **136**, 48-65.

Nordstrom, D. K. and Archer, D. G. (2003) Arsenic thermodynamic data and environmental geochemistry. In: Welch, A. H. and Stollenwerk, K. G. (Eds.), *Arsenic in Goundwater*. Kluwer, Boston.

O'Day, P. A., Rivera, N., Root, R., and Carroll, S. A. (2004a) X-ray absorption spectroscopic study of Fe reference compounds for the analysis of natural sediments. *Am. Mineral.* **89**, 572-585.

O'Day, P. A., Vlassopoulos, D., Root, R., and Rivera, N. (2004b) The influence of sulfur and iron on dissolved arsenic concentrations in the shallow subsurface under changing redox conditions. *Proc. Natl. Acad. Sci. U. S. A.* **101**, 13703-13708.

Oremland, R. S., Newman, D. K., Kail, B. W., and Stolz, J. F. (2002) Bacterial respiration of arsenate and its significance in the environment. In: Frankenberger, W. T., Jr. (Ed.), *Environmental Chemistry of Arsenic*. Marcel Dekker, Inc., New York.

Rickard, D. (1969) The chemistry of iron sulphide formation at low temperatures. *Stockholm Contributions in Geology* **20**, 67-95.
Rickard, D. (1997) Kinetics of pyrite formation by the H2S oxidation of iron (II) monosulfide in aqueous solutions between 25 and 125 degrees C: The rate equation. *Geochim. Cosmochim. Acta* **61**, 115-134.
Rickard, D. and Luther, G. W. (2007) Chemistry of iron sulfides. *Chem. Rev.* **107**, 514-562.
Root, R. A., Dixit, S., Campbell, K. M., Jew, A. D., Hering, J. G., and O'Day, P. A. (2007) Arsenic sequestration by sorption processes in high-iron sediments. *Geochim. Cosmochim. Acta* **71**, 5782-5803.
Root, R. A., Vlassopoulos, D., Rivera, N. A., Rafferty, M. T., Andrews, C., and O'Day, P. A. (2009) Speciation and natural attenuation of arsenic and iron in a tidally influenced shallow aquifer. *Geochim. Cosmochim. Acta* **73**, 5528-5553.
Stolz, J. F. and Oremland, R. S. (1999) Bacterial respiration of arsenic and selenium. *Fems Microbiol. Rev.* **23**, 615-627.
Uda, M. (1967) Structure of synthetic Fe3S4 and nature of transition to FeS. *Z. Anorgan. Allgem. Chem.* **350**, 105-&.
Vlassopoulos, D., Bessinger, B., and O'Day, P. A. (2010) Aqueous solubility of As2S3 and thermodynamic stability of thioarsenites. *Water-Rock Interaction Conference Proceedings*, Mexico.
Webb, S. M. (2005) SIXPack: a graphical user interface for XAS analysis using IFEFFIT. *Phys. Scr.* 4.
Webb, S. M. (2006) SMAK:Sam's Microprobe Analysis Kit. Stanford Synchrotron Radiation Lightsource, Stanford.
Wei, D. W. and OsseoAsare, K. (1996) Particulate pyrite formation by the Fe3+/HS- reaction in aqueous solutions: Effects of solution composition. *Colloids and Surfaces a-Physicochemical and Engineering Aspects* **118**, 51-61.
Yamaguch, S. and Wada, H. (1972) Aging of colloidal iron sulfide. *J. Colloid Interface Sci.* **40**, 477.

Table 1. Summary of precipitation experiments.

Experiment #		Species	Reagent source	Reagent salt	Molar ratio	pH[a]	Temp. °C	Equil. time (d)	Ref. [c]
1. End-member As-Sulfides ($As^{3+} + S^{2-}$)	1.1.	As^{3+}	Reagent grade, Ricca Chemical	$NaAsO_2$	1:1.7 As^{3+}:S^{2-}	4	25	1	1
		S^{2-}	ACS grade, Acros Organics	$Na_2S{\cdot}9H_2O$					
2. End-member Fe-Sulfides (Fe^{2+} or $Fe^{3+} + S^{2-}$)	2.1.	Fe^{2+}	ACS grade, J.T. Baker	$Fe(NH_4)_2(SO_4)_2{\cdot}6H_2O$	1:1 Fe^{2+}:S^{2-}	6, 8[b]	25, 60, 100	0.2, 7	2, 3
		S^{2-}	ACS grade, Acros Organics	$Na_2S{\cdot}9H_2O$					
	2.2.	Fe^{2+}	ACS grade, J.T. Baker	$Fe(NH_4)_2(SO_4)_2{\cdot}6H_2O$	1:2 Fe^{2+}:S^{2-}	5, 6	100, 190	7	4, 5
		S^{2-}	ACS grade, Acros Organics	$Na_2S{\cdot}9H_2O$	0.8:1 Fe^{2+}:S^{2-}		quench		
	2.3.	Fe^{2+}	ACS grade, Fisher Chemical	$FeSO_4{\cdot}7H_2O$	1:1.3:0.8 Fe^{2+}:S^{2-}:S	4, 6, 8	25	7	6
		S^{2-}	Alfa Aesar	Na_2S					
		S	99.98% trace metal basis, Sigma A.	Sulfur powder					
	2.4.	Fe^{2+}	99.0% puriss, p.a., Sigma Aldrich	$FeCl_2{\cdot}4H_2O$	1:1 Fe^{2+}:S^{2-}	6, 8	25	7	7
		S^{2-}	ACS grade, Acros Organics	$Na_2S{\cdot}9H_2O$					
	2.5.	Fe^{2+}	99.0% puriss, p.a., Sigma Aldrich	$FeCl_2{\cdot}4H_2O$	1:2 Fe^{2+}:S^{2-}	3	25	7	6
		S^{2-}	ACS grade, Acros Organics	$Na_2S{\cdot}9H_2O$					
	2.6.	Fe^{3+}	ACS grade, Fisher Chemical	$FeCl_3{\cdot}6H_2O$	1:2 Fe^{3+}:HS^-	4	25	7	8
		HS^-	Acros Organics	$NaHS{\cdot}xH_2O$					
	2.7.	Fe^{3+}	ACS grade, Fisher Chemical	$FeCl_3{\cdot}6H_2O$	1:1 Fe^{3+}:S^{2-}	6, 8	25	7	8
		S^{2-}	ACS grade, Acros Organics	$Na_2S{\cdot}9H_2O$	1:2 Fe^{3+}:S^{2-}	3			

3. Serial Batch (SB) Experiments (As^{3+} + S^{2-} + Fe^{2+} or Fe^{3+})	3.1.	As^{3+} S^{2-} Fe^{2+}	Reagent grade, Ricca Chemical ACS grade, Acros Organics ACS grade, J.T. Baker	$NaAsO_2$ $Na_2S \cdot 9H_2O$ $Fe(NH_4)_2(SO_4)_2 \cdot 6H_2O$	1:1:0.7 Fe^{2+}:S^{2-}:As^{3+}	4, 6, 8	25	7, 30	9
	3.2.	As^{3+} HS^- Fe^{3+}	Reagent grade, Ricca Chemical Acros Organics ACS grade, Fisher Chemical	$NaAsO_2$ $NaHS \cdot xH_2O$ $FeCl_3 \cdot 6H_2O$	0.5:1:0.6 Fe^{3+}:S^{2-}:As^{3+}	4, 6, 8	25	7, 30	9
4. Large Volume Reactor (LVR) (As^{3+} + S^{2-} + Fe^{2+} or Fe^{3+})	4.1.	As^{3+} S^{2-} Fe^{2+}	Reagent grade, Ricca Chemical ACS grade, Acros Organics 99.0% puriss, p.a., Sigma Aldrich	$NaAsO_2$ $Na_2S \cdot 9H_2O$ $FeCl_2 \cdot 4H_2O$	1:1:0.7 Fe^{2+}:S^{2-}:As^{3+}	6, 8	25	7, 120, 210	9
	4.2.	As^{3+} S^{2-} Fe^{3+}	Reagent grade, Ricca Chemical ACS grade, Acros Organics ACS grade, Fisher Chemical	$NaAsO_2$ $Na_2S \cdot 9H_2O$ $FeCl_3 \cdot 6H_2O$	1:1:0.7 Fe^{2+}:S^{2-}:As^{3+}	6, 8	25	7, 120, 210	9

[(a)] pH adjustment by addition of HCl or NaOH.
[(b)] pH buffered with either MES (pK_a=6.15) or TRIS (pK_a=8.06) (obtained from Acros Organics) rather than HCl or NaOH.
[(c)] References (1) (Eary, 1992); (2) (Arakaki and Morse, 1993); (3) (Rickard, 1997); (4) (Uda, 1967); (5) (Yamaguch and Wada, 1972); (6) (Rickard, 1969); (7) (Gallegos et al., 2007); (8) (Wei and OsseoAsare, 1996); (9) this study.

Table 2. Iron EXAFS fit results for end-member precipitates and SB and LVR experiments.

							Crystallographic Values		
							Mackinawite (FeS)[a]		
Experiment	Atom	N	R (Å)	σ^2 (Å^2)	ΔE_0 (eV)	χ^2	Atom	N	R (Å)
End-member	S	4.3*	2.24*	0.0046	−5.0	2.4	S	4	2.255
2.1: Fe^{2+} + S^{2-}	Fe	3.2*	2.60*	0.0069			Fe	4	2.598
0.2 d, pH 6	Fe	4.2*	3.66*	0.0130			Fe	4	3.674
End-member	S	4	2.24	0.0026*	−2.8	3.8	S	8	4.311
2.1: Fe^{2+} + S^{2-}	Fe	4	2.61	0.0038*					
7 d, pH 6	Fe	4	3.67	0.0070*					
	S	8	4.29	0.0063*			Pyrite (FeS_2)[b]		
End-member	S	6	2.25	0.0021*	−5.5	4.5	S	6	2.2566
2.7: Fe^{3+} + S^{2-}	S	6	3.46	0.0035*			S	6	3.4449
pH 3	Fe	12	3.84	0.0050*			Fe	12	3.8212
End-member	S	1.9*	2.29*	0.0026	−0.6	1.0			
2.7: Fe^{3+} + S^{2-}	Fe	1.5*	2.72*	0.0038					
pH 6	O	2.5*	2.05*	0.0040	1.3				
SB 3.1: As^{3+} +	S	1.0*	2.31*	0.0026	−0.6	0.5			
Fe^{2+} + S^{2-}	Fe	1.1*	2.73*	0.0038					
7 d, pH 6	O	3.7*	2.07*	0.0040	1.3				
LVR 4.1: As^{3+}	S	1.0*	2.28*	0.0026	0.5	0.4			
+ Fe^{2+} + S^{2-}	Fe	0.8*	2.67*	0.0038					
210 d, pH 6	O	3.1*	2.10*	0.0040	2.8				
	Fe	2.6*	3.22*	0.0052					
	S	2.0*	2.27*	0.0026	−3.9	0.5			
LVR 4.1.	Fe	1.5*	2.71*	0.0038					
210 d, pH 8	O	1.8*	2.09*	0.0040	0.02				
	Fe	3.0*	3.23*	0.0052					
LVR 4.2: As^{3+}	S	1.3*	2.26*	0.0026	1.7	0.3			
+ Fe^{3+} + S^{2-}	Fe	1.3*	2.69*	0.0038					
210 d, pH 6	Fe	0.7*	3.50*	0.0052					
	O	3.6*	2.06*	0.0080	1.9				
	S	2.3*	2.26*	0.0026	-6.5	0.6			
LVR 4.2.	Fe	1.4*	2.68*	0.0038					
210 d, pH 8	O	2.1*	2.00*	0.0040	4.2				
	Fe	1.4*	3.12*	0.0090					

* Parameter varied in fit; either number of backscatterers (N) fixed on crystallographic values and Debye-Waller factor (σ^2) varied, or N varied and σ^2 fixed on values from (O'Day et al., 2004a) and (Root et al., 2007).

[a] Mackinawite crystal structure from (Lennie and Vaughan, 1996).

[b] Pyrite crystal structure from (Elliott, 1960).

Table 3. Arsenic EXAFS fit results for end-member precipitates and SB and LVR experiments.[a]

Experiment	Atom	*N	*R (Å)	σ^2 (Å^2)	*ΔE_0 (eV)	χ^2	Crystallographic Values for Orpiment (As_2S_3)[b] Atom	N	R (Å)
End-member	S	2.9	2.27	0.0026	−10	0.49	S	3	2.243-2.307
1.1: As^{3+} + S^{2-}	As	1.0	3.05	0.011			As	1	3.191
1 d, pH 4	S	1.0	3.17	0.015			S	1	3.219, 3.291
	S	1.0	3.47	0.016			S	1	3.475, 3.514
	As	1.0	3.56	0.0057			As	1	3.521
SB 3.1: As^{3+} +	S	2.6	2.27	0.0026	−9.1	0.54	As	1	3.568
Fe^{2+} + S^{2-}	As	0.9	3.07	0.011					
30 d, pH 4	S	0.9	3.16	0.015					
	S	0.9	3.43	0.016					
	As	0.9	3.50	0.0057					
	O	1.2	1.79	0.0040	2.1	0.47			
SB 3.1:	S	1.5	2.27	0.0026	−9.5				
7 d, pH 6	As	0.5	3.06	0.011					
	S	0.5	3.19	0.015					
	S	0.5	3.49	0.016					
	As	0.5	3.58	0.0057					
LVR 4.1: As^{3+}	O	1.0	1.79	0.0040	−4.6	0.49			
+ Fe^{2+} + S^{2-}	S	1.5	2.28	0.0026	−6.6				
7 d, pH 6	As	0.5	3.06	0.011					
	S	0.5	3.19	0.015					
	S	0.5	3.49	0.016					
	As	0.5	3.57	0.0057					
	O	1.2	1.79	0.0040	1.3	0.69			
LVR 4.1.	S	1.6	2.27	0.0026	−9.7				
120 d, pH 6	As	0.5	3.06	0.011					
	S	0.5	3.19	0.015					
	S	0.5	3.49	0.016					
	As	0.5	3.58	0.0057					
	O	0.9	1.78	0.0040	3.1	0.75			
LVR 4.1.$^-$	S	1.8	2.28	0.0026	−9.6				
120 d, pH 6	As	0.6	3.06	0.011					
NaH_2PO_4	S	0.6	3.20	0.015					
extracted	S	0.6	3.49	0.016					
	As	0.6	3.59	0.0057					

	Atom	*N	*R (Å)	σ^2 (Å^2)	*ΔE_0 (eV)	χ^2	Crystallographic Values for Realgar (AsS)[a] Atom	N	R (Å)
LVR 4.1.	O	1.4	1.78	0.0040	0.8		S	2	2.225-2.251
210 d, pH 6	S	2.1	2.28	0.0040	−8.6		As	1	2.565-2.579
	O	2.4	1.78	0.0040	−0.2	0.19	S	1	3.415-3.513
	Fe	0.9	3.28	0.0035			As	2.5	3.439-3.499
LVR 4.1.	S	0.4	2.27	0.0034	−5.9		As	0.5	3.562
7 d, pH 8	As	0.3	2.54	0.0048			As	0.75	3.624-3.627
	As	0.9	3.47	0.0057			S	0.75	3.570-3.617
	O	2.2	1.79	0.0040	−2.3	0.45	S	2.5	3.657-3.689
	Fe	0.9	3.29	0.0035					
LVR 4.1.	S	0.7	2.26	0.0034	−9.0				
120 d, pH 8	As	0.5	2.58	0.0048					
	As	1.4	3.48	0.0057					
	O	2.3	1.78	0.0040	−0.4	0.30			
	Fe	1.1	3.28	0.0035					
LVR 4.1.	S	0.6	2.25	0.0034	−4.4				
210 d, pH 8	As	0.5	2.57	0.0048					
	As	1.8	3.48	0.0057					
LVR 4.2: As^{3+}	O	1.9	1.79	0.0040	−0.6	0.47			
+ Fe^{3+} + S^{2-}	Fe	0.7	3.37	0.0031					
7 d, pH 6	S	0.6	2.26	0.0040	−7.4				
	O	2.6	1.78	0.0040	0.1	0.44			
LVR 4.2.	Fe	0.3	2.94	0.0031					
120 d, pH 6	Fe	0.7	3.38	0.0031					
	S	0.5	2.30	0.0040	−7.0				
	O	2.5	1.77	0.0040	−1.8	0.21			
LVR 4.2.	Fe	0.2	2.94	0.0031					
210 d, pH 6	Fe	0.6	3.35	0.0031					
	S	0.7	2.27	0.0040	−9.9				
	O	3.2	1.77	0.0040	0.1	0.37			
LVR 4.2.	Fe	0.4	2.94	0.0031					
210 d, pH 8	Fe	0.8	3.37	0.0031					

[a]*N, *R, and *E_0 varied in fits; σ^2 for Fe^{2+} LVR 210 d fits taken from(O'Day et al., 2004b) and σ^2 for Fe^{3+} LVR 210 d fits taken from (Root et al., 2009).
[b] Orpiment and realgar crystal structures from (Mullen and Nowacki, 1972).

Table 4. Linear combination fits for Iron XANES (data range: 7105 to 7135 eV).

Experiment	Equil. time (d)	pH	Iron Sulfide			Green Rust[a]			Fe(III) Oxide[a]			Total[b]
			Fit %	Energy-shift (eV)	Est. Std. Dev.	Fit %	Energy-shift (eV)	Est. Std. Dev.	Fit %	Energy-shift (eV)	Est. Std. Dev.	
$Fe^{2+} + S^{2-}$												
2.1	0.2	6	97[c]	0.5	0.002	–	–	–	–	–	–	97
2.1	7	6	88[c]	0.1	0.002	–	–	–	–	–	–	88
$As^{3+} + Fe^{2+} + S^{2-}$												
SB 3.1.	7	6	53[c]	0.6	0.011	42	0.5	0.009	–	–	–	95
LVR 4.1.	210	6	43[e]	0.1	0.005	40	0.5	0.005	–	–	–	83
LVR 4.1.	210	8	54[c]	0.2	0.007	31	0.2	0.005	–	–	–	85
$Fe^{3+} + S^{2-}$												
2.7	7	3	94[d]	0.3	0.008	–	–	–	–	–	–	94
2.7	7	6	75[c]	0.3	0.008	24	0.7	0.007				99
$As^{3+} + Fe^{3+} + S^{2-}$												
LVR 4.2.	210	6	44[c]	0.06	0.018	–	–	–	51[f]	1.1	0.017	95
LVR 4.2.	210	8	48[c]	0.4	0.022	–	–	–	59[f]	0.3	0.020	107

[a] Standards from (O'Day et al., 2004a).
[b] Fit results not recalculated to 100%.
[c] Fit with amorphous mackinawite.
[d] Fit with crystalline pyrite.
[e] Fit with crystalline mackinawite.
[f] Fit with hematite.

Table 5. Linear combination fits for Arsenic XANES (data range: 11865 to 11880 eV).

Experiment	Equil. time (d)	pH	As-sulfide			As^{3+}-Oxide			Total[(e)]
			Fit %	Energy-shift (eV)	Est. Std. Dev.	Fit %	Energy-shift (eV)	Est. Std. Dev.	
$As^{3+} + Fe^{2+} + S^{2-}$									
SB 3.1.	30	4	100[(a)]	0.1	0.01	–	–	–	100
SB 3.1.	7	6	88[(a)]	0.1	0.06	17[(c)]	0.3	0.05	105
LVR 4.1.	7	6	70[(a)]	0.5	0.03	25[(c)]	0.9	0.02	95
LVR 4.1.	120	6	64[(a)]	0.4	0.04	34[(c)]	0.0	0.03	98
LVR 4.1.	210	6	67[(a)]	0.0	0.05	31[(c)]	0.1	0.04	98
LVR 4.1.	7	8	15[(b)]	0.7	0.02	88[(c)]	0.5	0.02	103
LVR 4.1.	120	8	10 [(b)]	0.6	0.04	94[(c)]	0.5	0.03	104
LVR 4.1.	210	8	8 [(b)]	0.6	0.04	94[(c)]	0.4	0.04	102
$As^{3+} + Fe^{3+} + S^{2-}$									
LVR 4.2.	7	6	28[(a)]	0.0	0.02	71[(d)]	0.3	0.02	99
LVR 4.2.	120	6	21[(a)]	0.1	0.06	90[(d)]	0.1	0.06	111
LVR 4.2.	210	6	39[(a)]	0.3	0.04	71[(d)]	0.5	0.05	110
LVR 4.2.	210	8	–	–	–	101[(d)]	0.03	0.01	105

[(a)] Fit with amorphous orpiment (Root et al., 2009).
[(b)] Fit with crystalline realgar (O'Day et al., 2004b).
[(c)] Fit with As^{3+} sorbed to green rust (Root et al., 2007).
[(d)] Fit with As^{3+} sorbed to Fe(III)-oxide (Root et al., 2007).
[(e)] Fit results not recalculated to 100%.

Table 6. Linear combination fits for Sulfur XANES (data range: 2460 to 2490 eV).

Experiment	Equil. time (d)	pH	Orpiment (am)[a]			Realgar[b]			Mackinawite			Total[c]
			Fit %	Energy-shift (eV)	Est. Std. Dev.	Fit %	Energy-shift (eV)	Est. Std. Dev.	Fit %	Energy-shift (eV)	Est. Std. Dev.	
$As^{3+} + Fe^{2+} + S^{2-}$												
SB 3.1.	7	6	46	0.2	0.005	–	–	–	57[d]	0.3	0.005	103
LVR 4.1.	210	6	76	0.1	0.005	–	–	–	26[d]	0.3	0.005	102
LVR 4.1.	210	8	–	–	–	21	0.3	0.004	76[d]	0.3	0.004	97
$As^{3+} + Fe^{3+} + S^{2-}$												
SB 3.2.	7	4	101	0.3	0.003	–	–	–	–	–	–	101
LVR 4.2.	210	6	50	0.6	0.007	–	–	–	49[e]	0.2	0.007	99
LVR 4.2.	210	8	–	–	–	–	–	–	95[d]	0.2	0.004	95

[a] Fit with amorphous orpiment.
[b] Fit with crystalline realgar.
[c] Fit results not recalculated to 100%.
[d] Fit with crystalline mackinawite
[e] Fit with amorphous mackinawite.

Table 7. pH and ORP values for large-volume reactor (LVR) suspensions after 7 d and 120 d aging.

Experiment	Aging Time (d)	Initial pH	Final pH	ORP (mV)
LVR 4.1.	7	6	6.0	+ 33.0
	120	6	5.5	+ 71.0
$As^{3+} + Fe^{2+} + S^{2-}$	7	8	8.2	- 140
	120	8	8.6	- 103
LVR 4.2.	7	6	6.0	+ 40.0
	120	6	5.6	+ 72.0
$As^{3+} + Fe^{3+} + S^{2-}$	7	8	7.8	- 70.0
	120	8	7.6	- 68.5

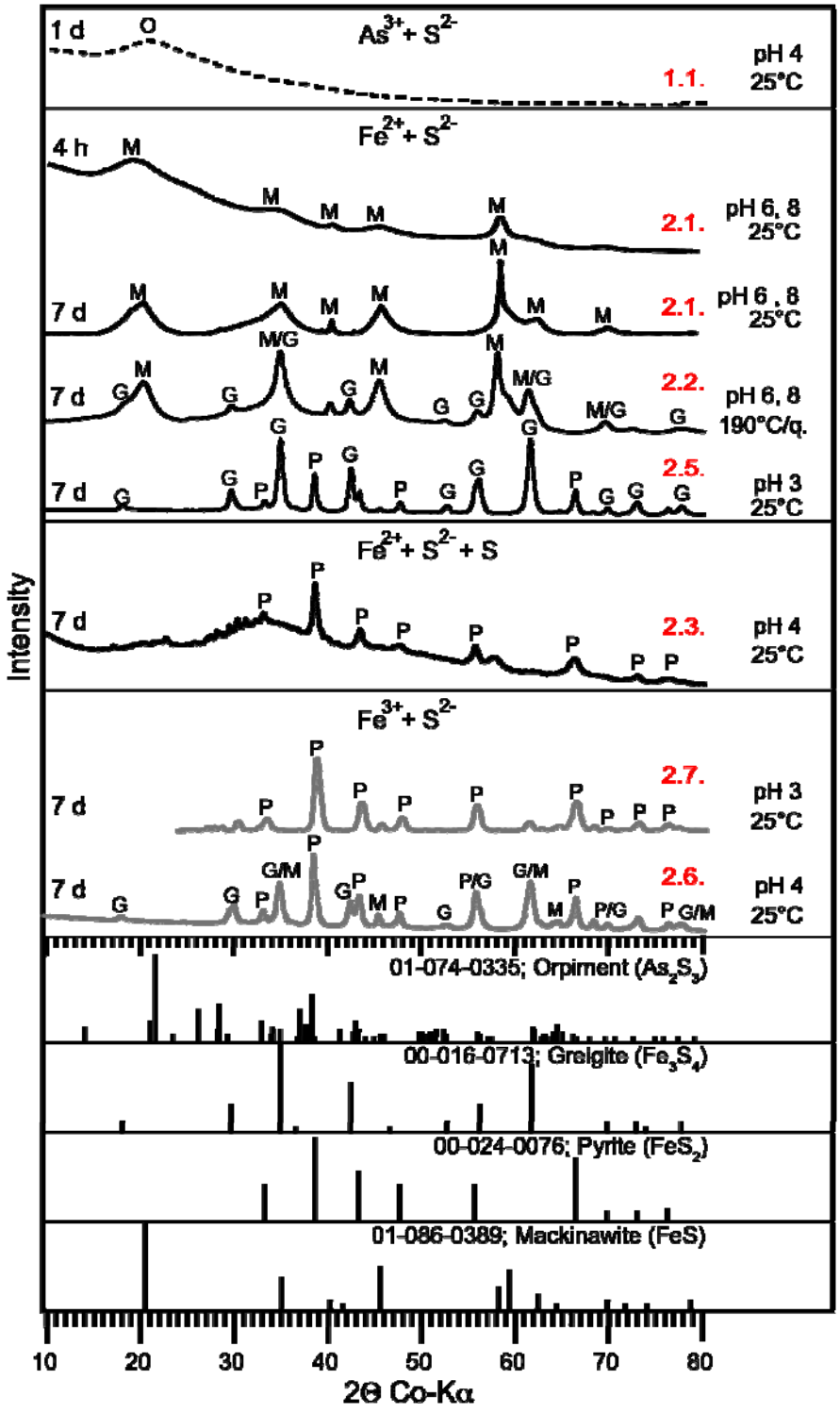

Figure 1. X-ray diffractograms of end-member precipitates. Key to experiment number given in Table 1.

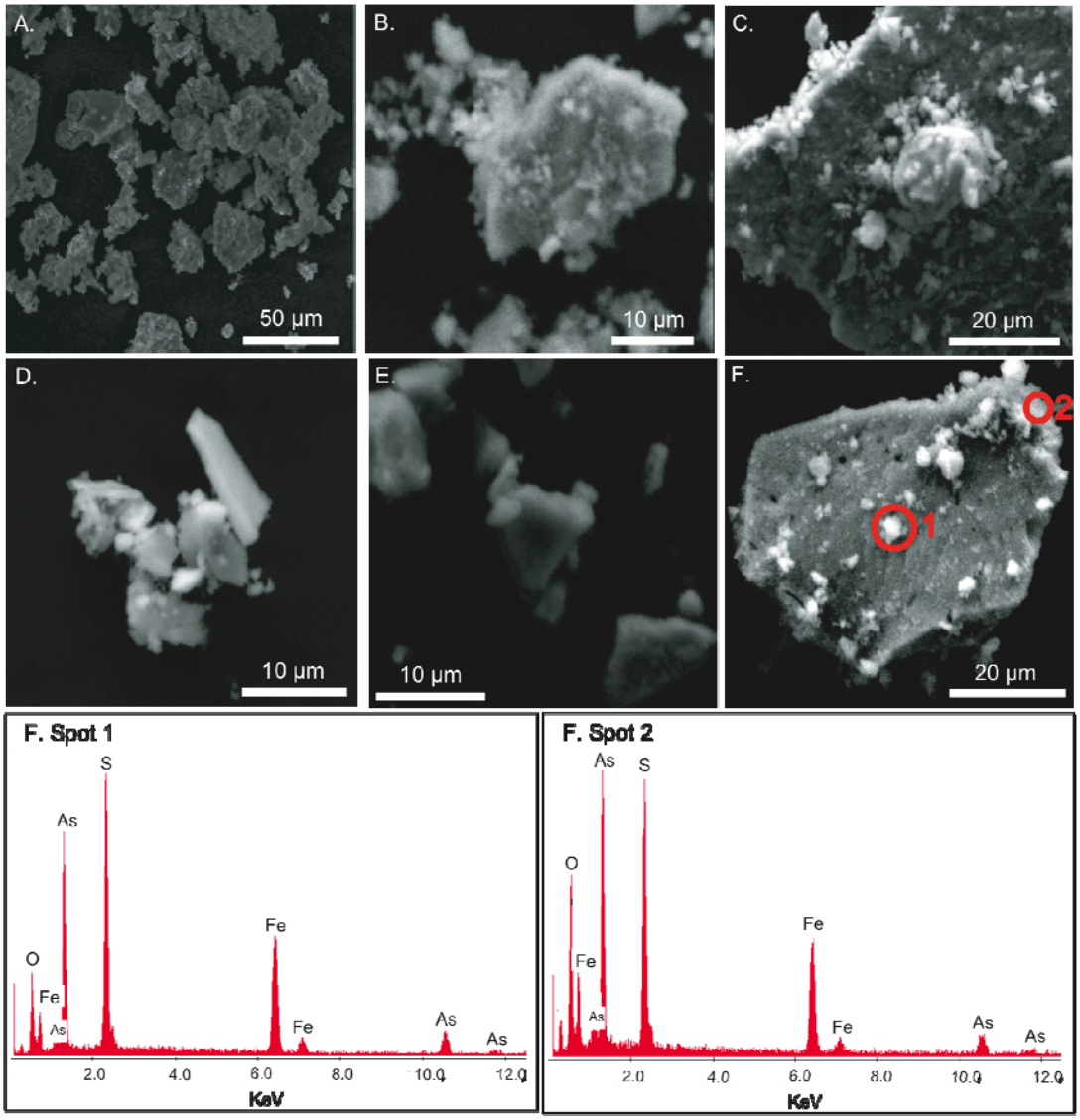

Figure 2. Scanning electron micrographs and energy dispersive spectrometry (EDS) of experimental precipitates. (A.) FeS (no As) aged 7 d, showing a typical morphology of mackinawite platelets. (B, C, D.) As^{3+}+Fe^{2+}+S^{2-} LVR precipitates aged 120 d. (E, F.) As^{3+}+Fe^{3+}+S^{2-} LVR precipitates aged 120 d. In B, C, and F, aggregates can be seen growing on surfaces of other aggregated particles, suggesting two different phases. (F.) Spots 1 and 2 EDS show the elemental components of these precipitates: As, Fe and S.

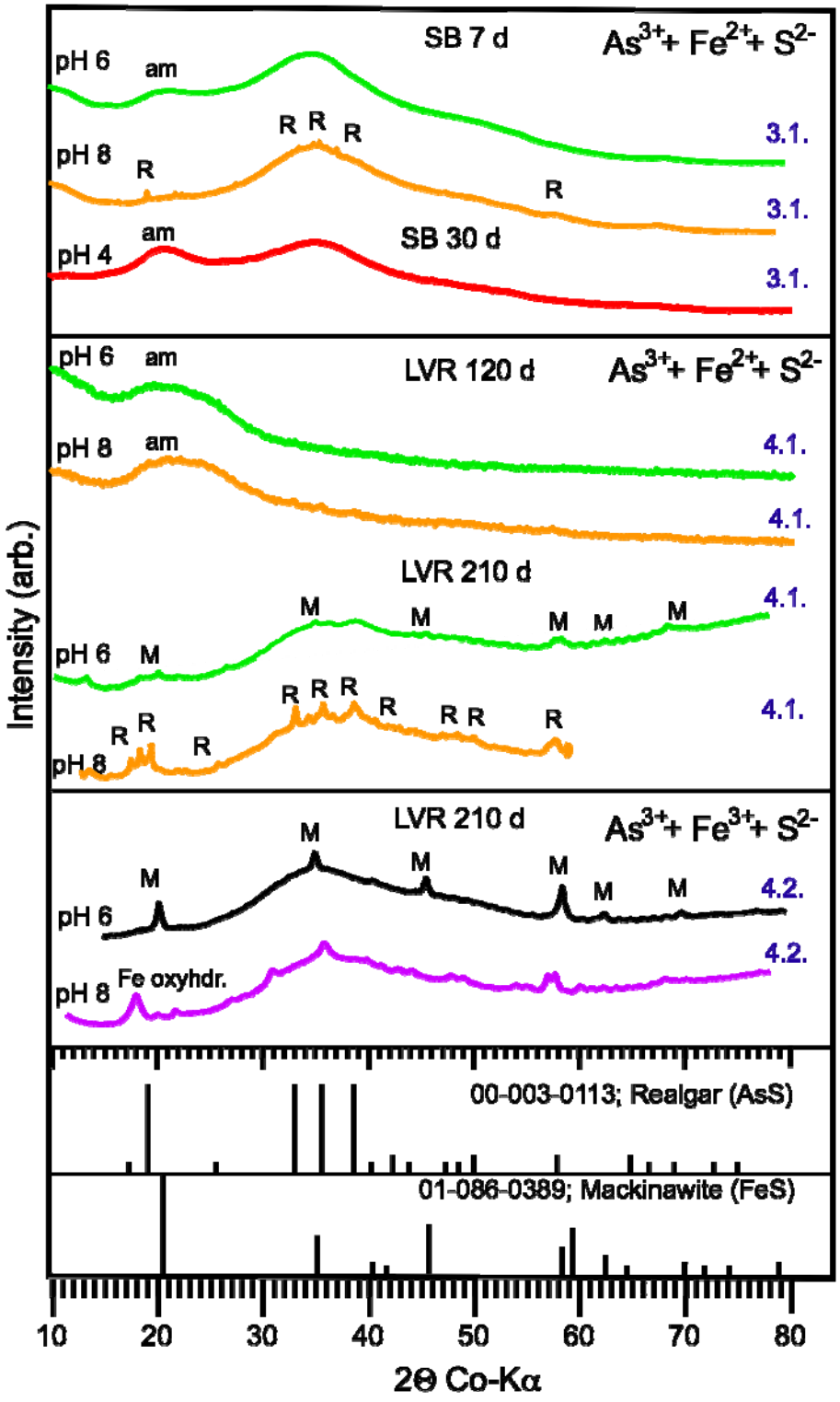

Figure 3. X-ray diffractograms of experimental precipitates from from starting solutions with $As^{3+} + Fe^{2+} + S^{2-}$ and $As^{3+} + Fe^{3+} + S^{2-}$. Key to experiment number given in Table 1.

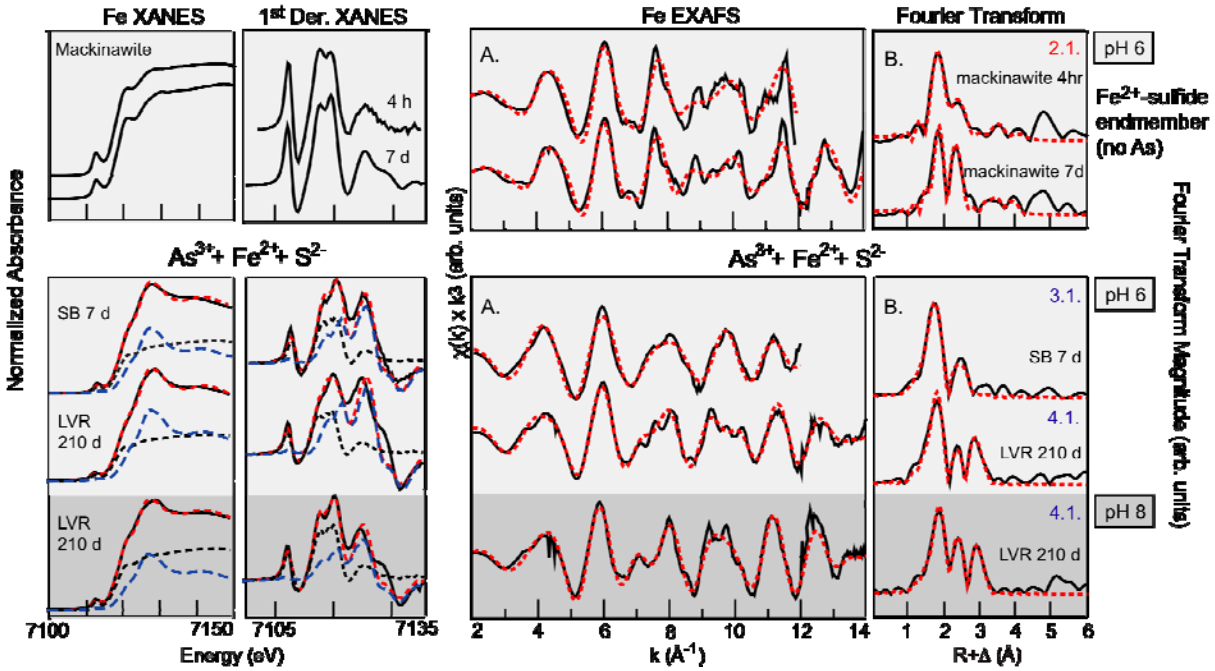

Figure 4. Iron X-ray absorption spectra of experimental precipitates from starting solutions with As^{3+} + Fe^{2+} + S^{2-}. Solid lines are experimental data; dashed lines are least-squares best fits. Numerical results for XANES fits tabulated in Table 4; numerical results for EXAFS fits tabulated in Table 2.

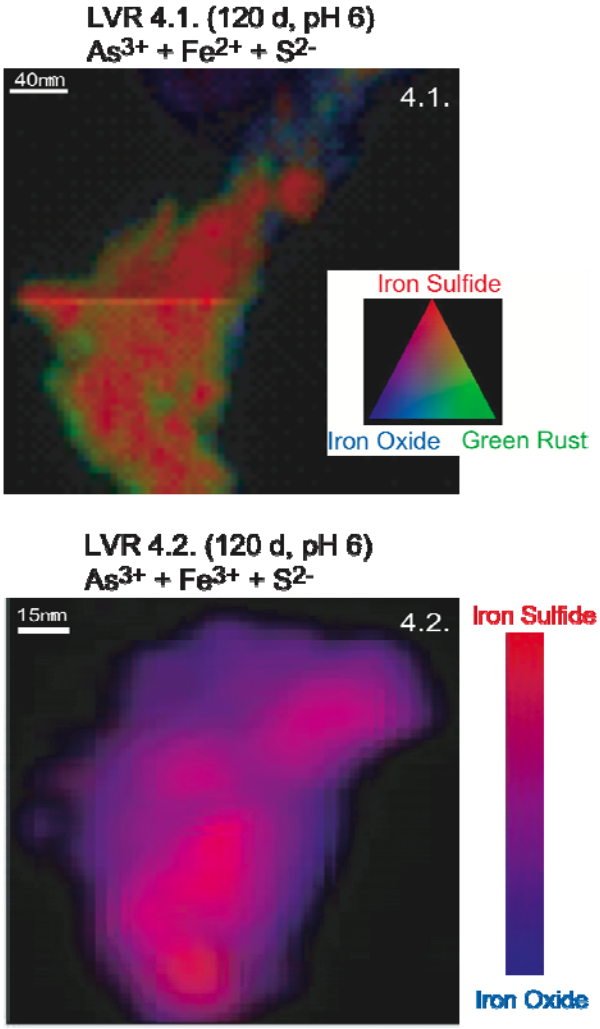

Figure 5. Microfocused synchrotron X-ray fluorescence energy difference maps for the Fe K-edge. The maps were constructed by scanning the particle at different energies (7113, 7126, 7129 and 7140 eV), which correspond to maximum absorption in the edge region for the different iron mineral phases indicated.

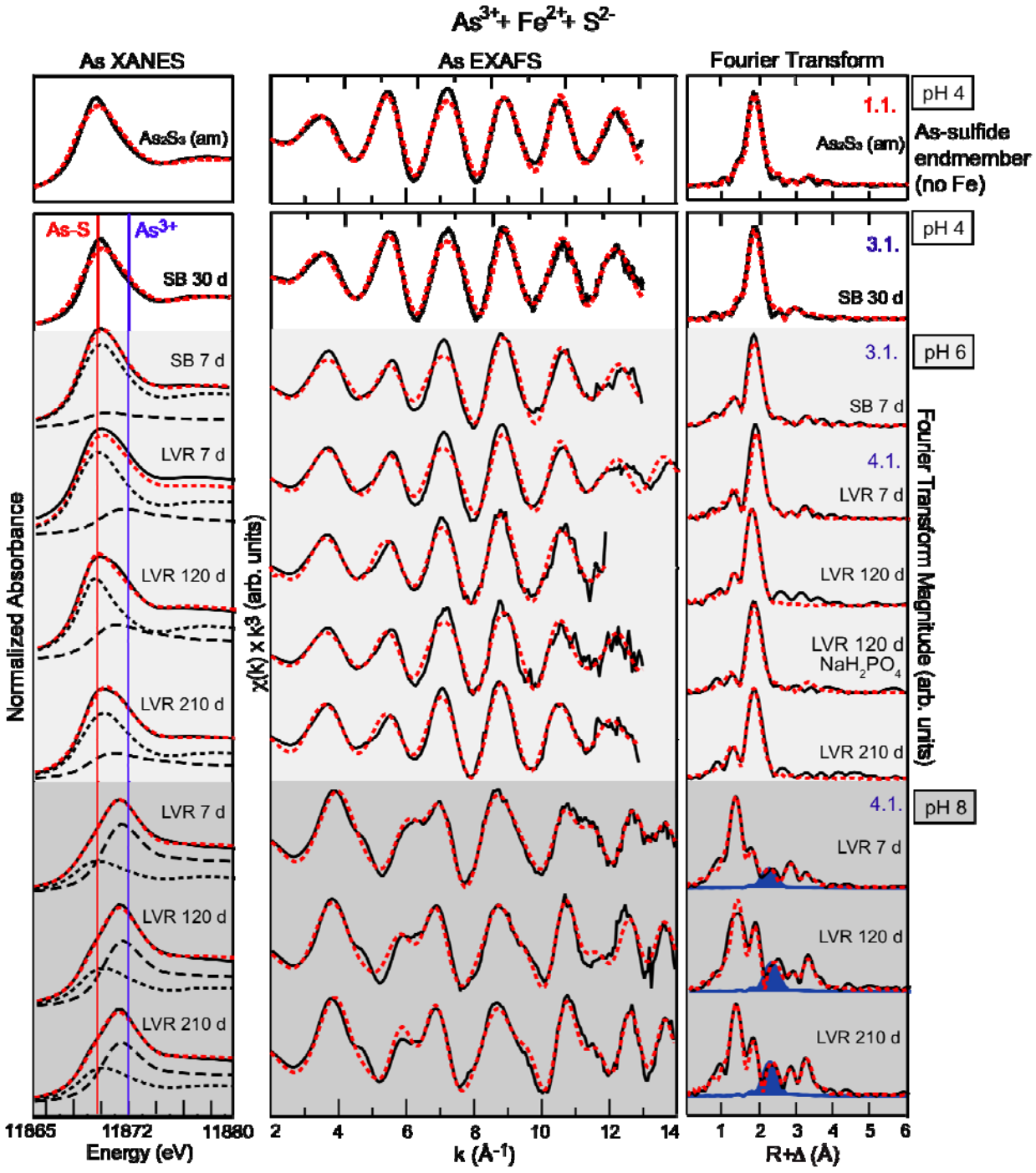

Figure 6. Arsenic X-ray absorption spectra of experimental precipitates from starting solutions with As^{3+} + Fe^{2+} + S^{2-}. Solid lines are experimental data; dashed lines are least-squares best fits. Numerical results for XANES fits tabulated in Table 5; numerical results for EXAFS fits tabulated in Table 3.

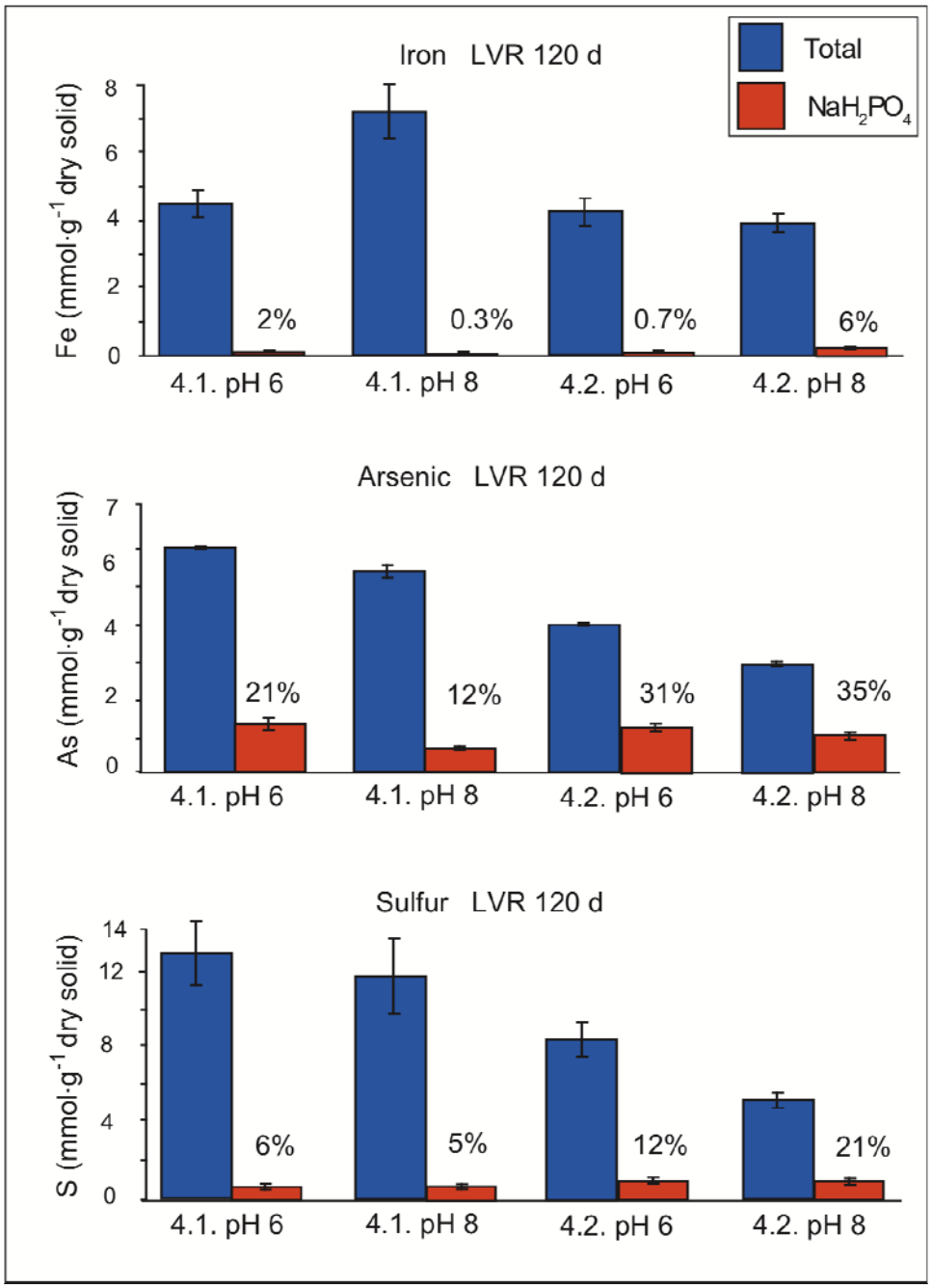

Figure 7. Extracted concentrations of Fe, As, and S compared to total concentrations from measurement of digested solids for LVR precipitates after 120 d of aging. Extraction solution was 0.005 M NaH_2PO_4. Concentrations normalized to total dry weight of solids.

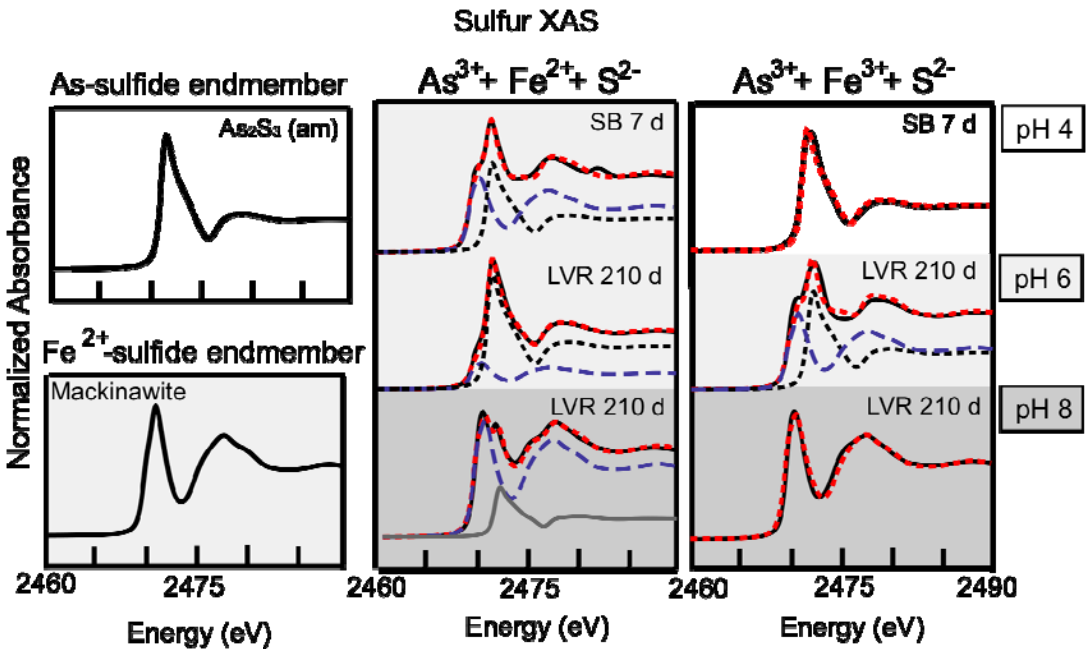

Figure 8. Sulfur X-ray absorption spectra of experimental precipitates from starting solutions with As^{3+} + Fe^{2+} + $S^{2-}$and As^{3+} + Fe^{3+} + S^{2-}, and Fe and As end members. Solid lines are experimental data; dashed lines are least-squares best fits. Numerical fit results tabulated in Table 6.

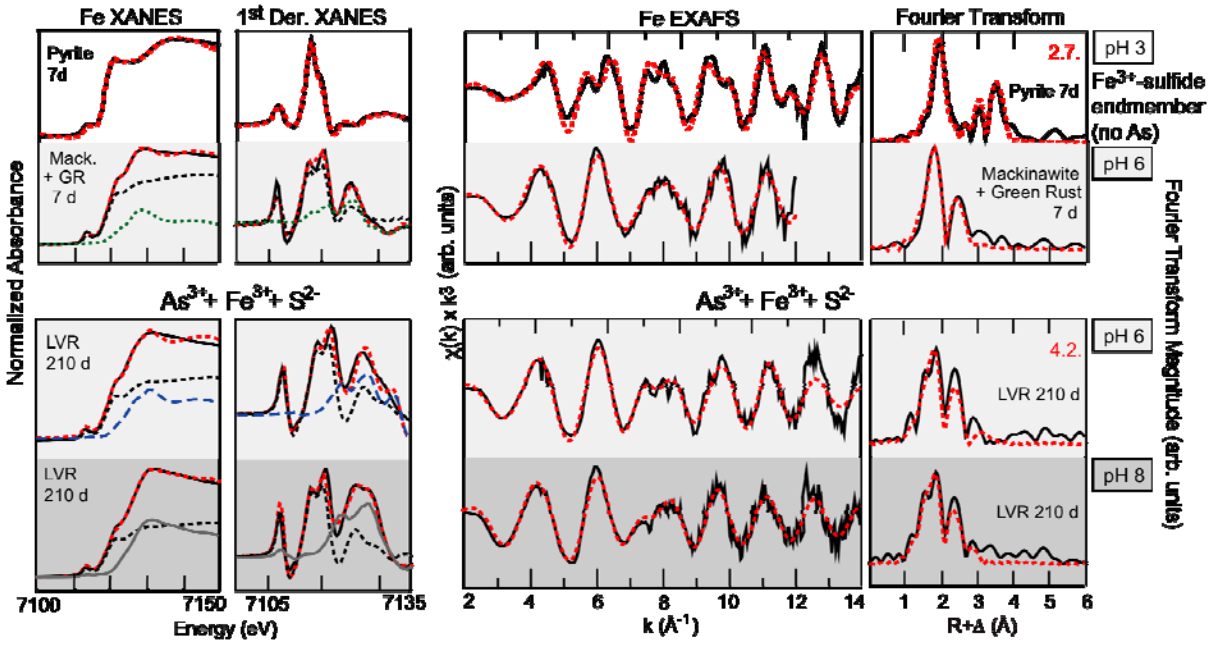

Figure 9. Iron X-ray absorption spectra of experimental precipitates from starting solutions with As^{3+} + Fe^{3+} + S^{2-}. Solid lines are experimental data; dashed lines are least-squares best fits. Numerical results for XANES fits tabulated in Table 4; numerical results for EXAFS fits tabulated in Table 2.

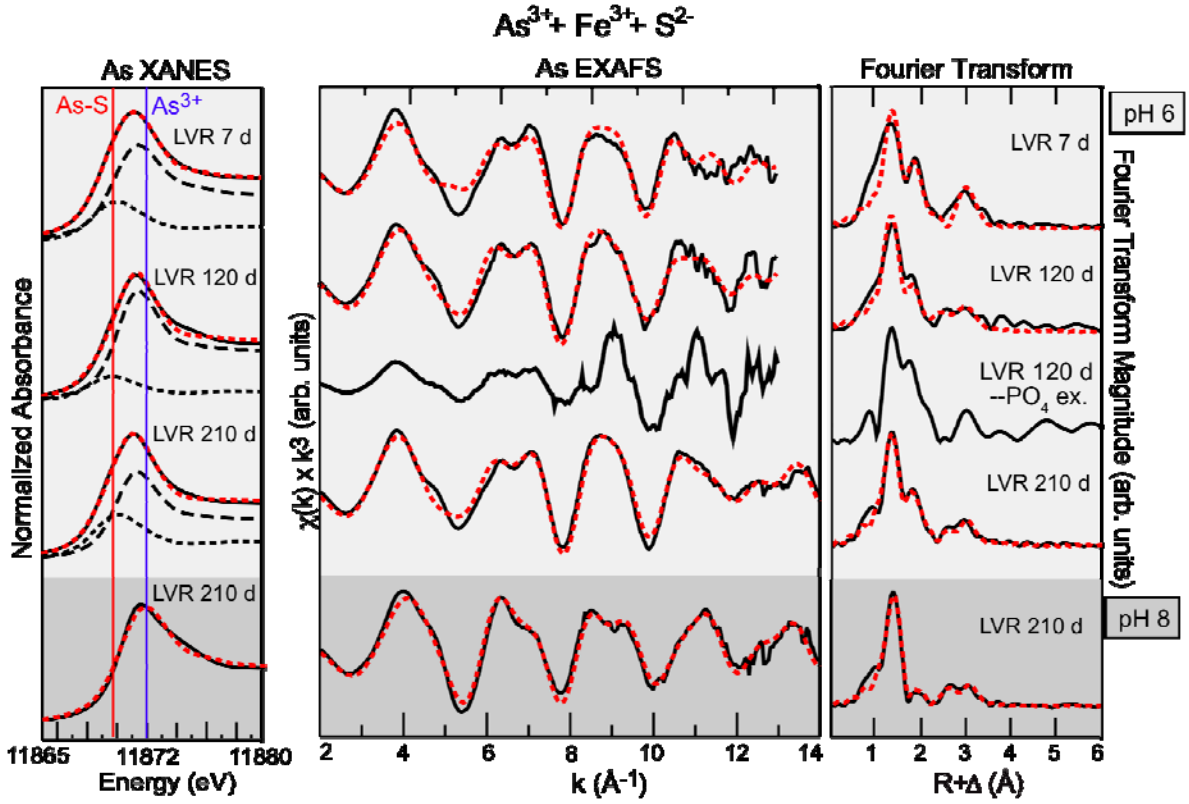

Figure 10. Arsenic X-ray absorption spectra of experimental precipitates from starting solutions with As^{3+} + Fe^{3+} + S^{2-}. Solid lines are experimental data; dashed lines are least-squares best fits. Numerical results for XANES fits tabulated in Table 5; numerical results for EXAFS fits tabulated in Table 3.

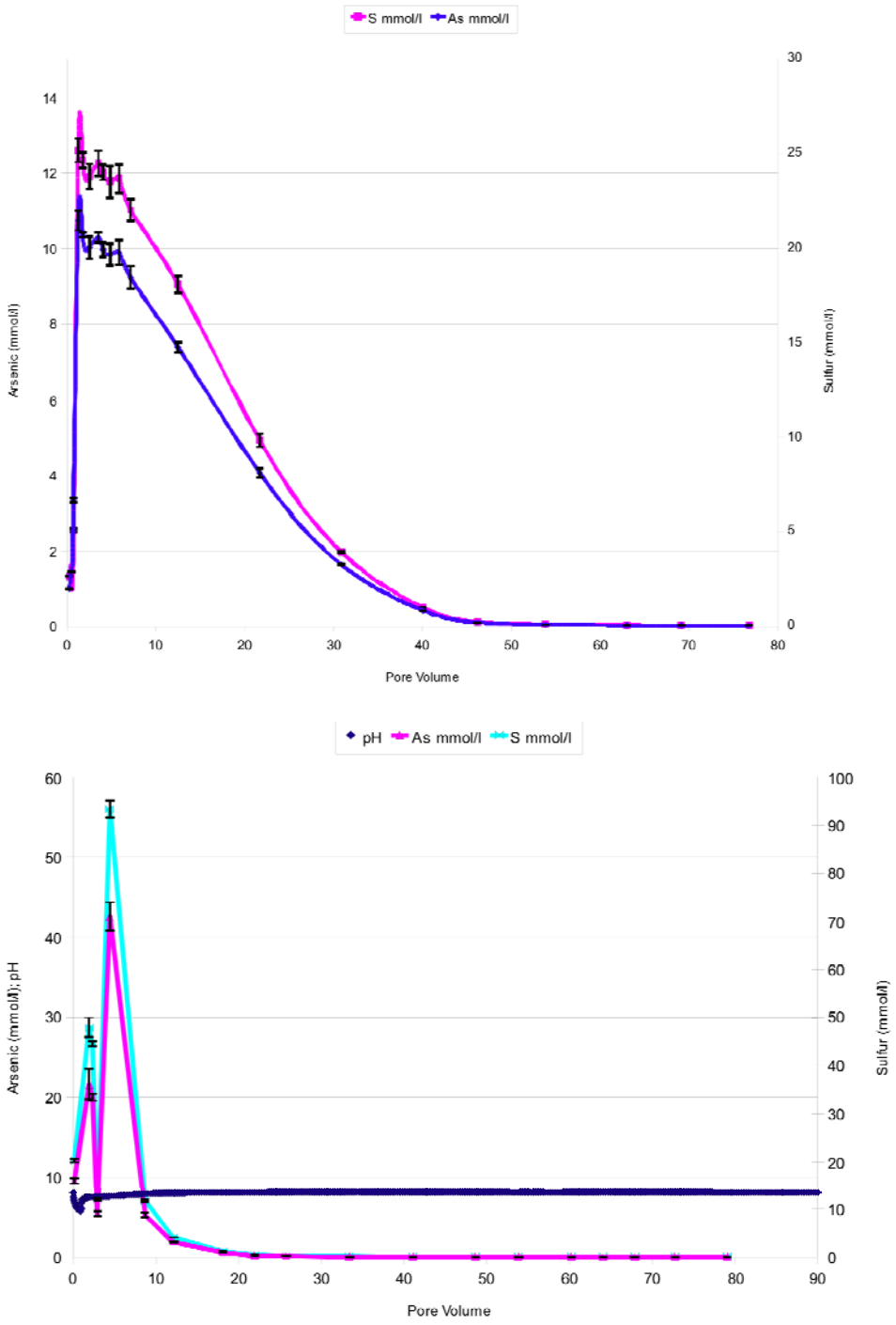

Figure 11. Total As and S in effluent solution in flow-through column dissolution experiments for amorphous As_2S_3(s) packed in an inert quartz matrix. Top: Influent solution: DO = 94%; pH 8 (Tris buffer). Bottom: Influent solution: DO = 0%; pH 8 (Tris buffer).

Appendices

Table A1. Total Fe, As, and S concentrations in solids from LVR 120 d experiments at pH 6 and 8 before and after washings (I, II and III), and concentrations measured in phosphate extractions of solids. Concentrations are normalized to total dry weight of the solids.

Experiment	pH	mmol Fe added to reactor[a]	g dry solid in reactor[b]	mmol Fe / g dry solid[c]				Phosphate-Extracted Conc.[d] (mmol Fe / g dry solid)
				Solid Conc. before Wash	Solid Conc. after Wash I	Solid Conc. after Wash II	Solid Conc. after Wash III	
LVR 4.1.	8	140	20	6.98	6.98	6.98	6.97	0.02
120 d	6	140	17	4.62	4.28	4.27	4.27	0.07
LVR 4.2.	8	126	28	4.45	4.44	4.29	4.05	0.25
120 d	6	126	25	4.40	4.32	4.32	4.31	0.03

Experiment	pH	mmol As added to reactor[a]	g dry solid in reactor[b]	mmol As / g dry solid[c]				Phosphate-Extracted Conc.[d] (mmol As / g dry solid)
				Solid Conc. before Wash	Solid Conc. after Wash I	Solid Conc. after Wash II	Solid Conc. after Wash III	
LVR 4.1.	8	109	20	5.25	5.18	5.13	5.04	0.61
120 d	6	109	17	6.03	5.95	5.91	5.87	1.23
LVR 4.2.	8	109	28	3.24	3.09	2.96	2.83	0.99
120 d	6	109	25	4.04	3.96	3.90	3.82	1.19

Experiment	pH	mmol S added[a] to reactor	g dry solid in reactor[b]	mmol S / g dry solid[c]				Phosphate-Extracted Conc.[d] (mmol S / g dry solid)
				Solid Conc. before Wash	Solid Conc. after Wash I	Solid Conc. after Wash II	Solid Conc. after Wash III	
LVR 4.1.	8	242	20	11.7	11.6	11.5	11.5	0.52
120 d	6	212	17	12.4	12.4	12.4	12.4	0.72
LVR 4.2.	8	212	28	5.61	5.14	5.10	5.04	1.06
120 d	6	212	25	8.33	8.29	8.27	8.16	1.01

[a] Total initial Fe, As and S added to LVR slurries (wet solid phase + supernatant). [b] Water content in precipitates ~ 85%. Dry solid was estimated based on measured water content. [c] Total Fe, As and S in the solid phase determined by difference (initial concentration – solution concentration) and recalculated to dry weight mass. Washes were in deoxygenated, deionized water. [d] Phosphate extraction was 0.005 M NaH_2PO_4.

B. List of Scientific/Technical Publications

Illera, V., Rivera, N. and O'Day, P. A. (2009) Spectroscopic characterization of co-precipitated arsenic- and iron-bearing sulfide phases at circum-neutral pH (abstract). *American Geophysical Union Annual Meeting,* Dec. 14-18, 2009 San Francisco, CA.

Illera, V., Rivera, N. and O'Day, P. A. (2010) Precipitation of arsenic sulfide phases at circum-neutral pH from Fe^{2+} and Fe^{3+} solutions (abstract). *American Chemical Society 239th Annual Meeting,* March 21-25, San Francisco, CA.